PRESSURE FLUCTUATIONS ON A SQUARE BUILDING MODEL IN BOUNDARY-LAYER FLOWS

A. KAREEM

University of Houston, Houston, TX 77004 (U.S.A.)

J.E. CERMAK

Colorado State University, Fort Collins, CO 80523 (U.S.A.)

Summary

Spatio—temporal measurements of a fluctuating pressure field acting on the side faces of a square prism of finite height in boundary-layer flows are presented for 0° angle of attack. Two typical neutral atmospheric flow conditions were simulated in the wind tunnel to represent open country and urban flow environments. The fluctuating pressure field data allowed computations of the mean and r.m.s. (root mean square) pressure coefficients, power spectral density, autocorrelations, co-spectra, cross-correlations, orthogonal eigenfunction expansions and statistical dependence. Increased levels of turbulence in the incident flow have a marked influence on the fluctuating pressure field, through modifications which take place in the structure of the separated shear layers. The periodic vortex-shedding process is vitiated in the presence of high levels of turbulence intensity in the incident flow, resulting in redistribution of the energy associated with pressure fluctuations over a wider frequency range.

Notation

B	building-model width
BL1	boundary layer 1
BL3	boundary layer 3
$C_{p\,\text{mean}}$	mean pressure coefficient
$C_{p_{\text{rms}}}$	r.m.s. pressure coefficient
$\text{Co}(g_1, g_2, n)/[S(g_1, n)\, S(g_2, n)]^{1/2}$	normalized co-spectra between locations g_1 and g_2
H	building-model height
n	frequency (Hz)
$P_i(x)$	probability-density histogram (PDF)
$P_{ij}(x, y)$	joint probability-density matrix (JPDF)
p	instantaneous pressure
$\bar{p}$	mean pressure
p_{static}	static pressure

Re	Reynolds number
$S(g_1, n)$	power spectrum at location g_1
U_h	mean longitudinal velocity at model height
$V(z)$	mean longitudinal velocity at z
$X1, X2$	locations of first and second pressure taps at various levels for chordwise correlations
$Z1, Z2$	locations of first and second pressure taps at various columns for spanwise correlations
ρ	air density
υ	coefficient of viscosity
δ	boundary-layer thickness
σ^2	mean square value
σ	r.m.s. value
$\hat{\sigma}_P$	normalized deviation between product of PDF's and JPDF
α	velocity-profile exponent

1. Introduction

The pressure fluctuations on the surface of a building exposed to an atmospheric boundary layer result from the turbulence present in the approach flow, from flow separation and reattachment, from vortex shedding in the wake, from building motion and from possible impingement of vortices shed by upstream objects. Successful analytical prediction of wind loads has been impaired by the complex nature of wind—structure interactions. Therefore, scale-model tests of buildings in simulated boundary-layer flows continue to serve as the most practical and promising means of predicting aerodynamic loads on structures.

Historically, there have been a number of investigations attempting to determine the overall mean and fluctuating drag and lift forces acting on prismatic bluff bodies and the mean and fluctuating pressures at various locations on the surface of bluff bodies. However, few studies have been made involving measurements of the spatio-temporal characteristics of the fluctuating pressure field. Vickery [1], Chaplin [2], Wilkinson [3], Lee [4] and Miyata and Miyazaki [5] measured steady and unsteady surface pressures and spatial correlations in two-dimensional flows. Vickery [1] presented measurements of the fluctuating lift and drag on a long square prism, including the spanwise and chordwise correlations. Vickery also obtained load spectra from force dynamometer measurements in uniform flow at 0° approach angle. The energy associated with the fluctuating lift force component was found primarily in a narrow band centered on the Strouhal frequency. Vickery concluded that the magnitudes of the steady and fluctuating forces acting on a long square prism are influenced markedly by the

presence of large-scale turbulence; the effects include an increase in the wake pressure and a reduction in the fluctuating lift force.

An extensive study of the effects of upstream turbulence on the pressure field of a square prism in two-dimensional flow was conducted by Lee [4]. Lee measured the steady and unsteady pressures and their spatial correlations, and derived spectra for a number of orientations in various approach flows with a wide range of turbulence intensities. Using eigenfunction expansions of the covariance matrices he concluded that the fundamental eigenvector, which represents the vortex-shedding mode, contained the highest percentage of energy. However, this percentage was reduced when the turbulence intensity of the approach flow was increased. Akins [6] carried out comprehensive measurements of pressure fluctuations to organize pressure measurements systematically for a wide range of buildings and boundary layers in order to isolate relevant geometrical and meteorological variables which affect the surface pressures on buildings.

Simplified studies conducted in smooth and turbulent flows over two-dimensional prisms provide qualitative insight into the individual importance of various flow characteristics, i.e., the effects of turbulence intensity and scale on pressure fluctuations. Furthermore, these studies add to the understanding of more complex flow fields and the associated pressure fluctuations on buildings in atmospheric wind. One of the major drawbacks in experiments performed in two-dimensional flows is the lack of three-dimensional flow characteristics. The influx of fluid from the top of a finite prism causes considerable disruption of the vortex-shedding process over the top portion of the prism. Therefore, the flow over the top of prisms with low aspect ratio will tend to increase the base pressure and reduce the pressure correlation, and thereby result in a reduction in the lift force. Another significant parameter among the approach-flow characteristics is the presence of shear, which contains distributed vorticity whose vector is perpendicular both to the stream and to the axis of the prism. On approaching a prism the vorticity vector "wraps itself around" the prism, until it approaches a streamwise direction. Vortex shedding occurs at different frequencies in cells of finite spanwise length; consequently, the pressure field on the side faces of a prism is less correlated. Therefore, the absence of a mean velocity gradient leads to higher spatial correlations, and consequently to higher values of the lift force. Inasmuch as the nature of the flow field about a building in atmospheric wind differs from the flow past a two-dimensional prism, careful interpretation of the results obtained from such studies is necessary.

In this study spatio-temporal pressure fluctuations were measured on the side faces of a square building model immersed in simulated boundary layers. The effects of an increase in the turbulence intensity of the approach flow were studied experimentally in order to assess the sensitivity of wind loads to changes in atmospheric turbulence. In addition to broadening knowledge in the field of wind loads on structures, insight was gained into the basic aerodynamics of flow past finite square prisms immersed in turbulent shear flows.

2. Experimental

All measurements were made in the industrial aerodynamics wind tunnel at Colorado State University. Similarity requirements for simulating a turbulent boundary layer in a wind tunnel were obtained from dimensional arguments derived from analytical relations describing the flow [7]. Turbulent boundary layers were generated by the natural action of the surface roughness of the tunnel floor and by upstream spires, providing what is generally considered to be reasonable simulation of the atmospheric boundary layer under neutrally stable conditions.

2.1. Details of model

A 5-inch square and 20-inch tall model made of Lucite was used for this study. The model was instrumented on two faces. A typical pressure tap was 0.06 inches in diameter and normal to the building face. Flexible Tygon tubing of short length was used to connect the pressure transducers to the pressure taps. The frequency response of the transducer—tube combinations was almost flat to 60 or 70 Hz, encompassing the range of pressure fluctuation frequencies containing significant information. The locations of the taps are shown in Fig. 1 and all the taps have counterparts directly opposite.

A typical tap location is represented by a number in the form S-L-C, where S indicates the prism side number, L the level on a side (numbered from top to bottom), and C the column.

2.2. Details of boundary-layer simulation

The boundary-layer wind tunnel used for these experiments has a test section 60 feet long with a ceiling whose height is adjustable from 5 to 7 feet. All pressure measurements were conducted for two approach flows, boundary layers 1 and 3, with the prism model mounted on a turntable with a large inertial mass at the downwind end of the long test section. Boundary layers 1 and 3 are referred to as BL1 and BL3 in this paper for convenience. Flow over the floor of the test section was used to generate BL1, whereas for BL3 the floor was covered with 2-inch randomized roughness-cubes [6, 8]. A set of spires and a horizontal barrier at the entrance of the test section were used in addition to the surface roughness to stimulate boundary-layer growth. The boundary layers BL1 and BL3 represent open country and urban flow conditions, respectively [8].

2.3. Details of measurement configurations

All measurements were conducted on two side faces, with the flow parallel to these faces. The model was divided into six levels at various heights. At each level, pressure was monitored at four locations on either side face simultaneously, to develop the chordwise pressure distribution. Similarly, pressure was monitored along four vertical axes on the side faces to establish the spanwise pressure distribution. A total of thirteen configurations were measured for each flow condition.
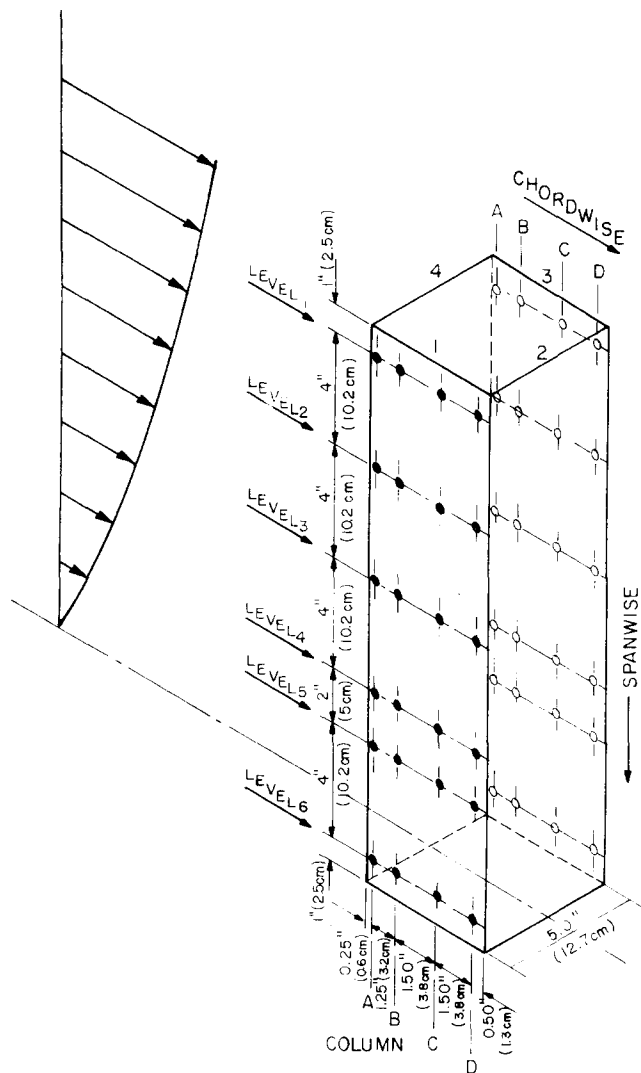
Fig. 1. Locations of pressure taps on side faces.

2.4. Details of instrumentation, data acquisition and reduction

The output from the pressure transducers was fed through a signal-conditioning unit for amplification. A constant-temperature hot-film anemometer was used to measure the characteristics of the boundary-layer flows. An on-line digital data-acquisition system was employed for simultaneous monitoring of eight channels of pressure data. The important components of the instrumentation system are an analog-to-digital converter, a minicomputer and a digital tape-recorder. Time histories of the pressure fluctuations were measured and recorded on digital tapes for a duration of 300 s at 500 samples/s [8, 9].

Using methods of digital time-series analysis for reduction of the measured pressure data, the following spectral and statistical characteristics were derived from the measurements: (a) autocorrelation and cross-correlation; (b) power and co-spectral density functions; (c) orthogonal eigenfunction expansion; (d) correlation length scale; and (e) statistical dependence.

3. Experimental results

The mean-velocity and local turbulence-intensity profiles as functions of nondimensional height are presented in Fig. 2 for the BL1 and BL3 flows, respectively (all tests were conducted at Re $(= U_h B/v)$ of 1.1×10^5).

Mean and r.m.s. pressure coefficients, based on the mean wind speed at model height, were computed for the BL1 and BL3 flows. The more significant results (representing levels 2 and 3) are presented in Figs. 3 and 4.
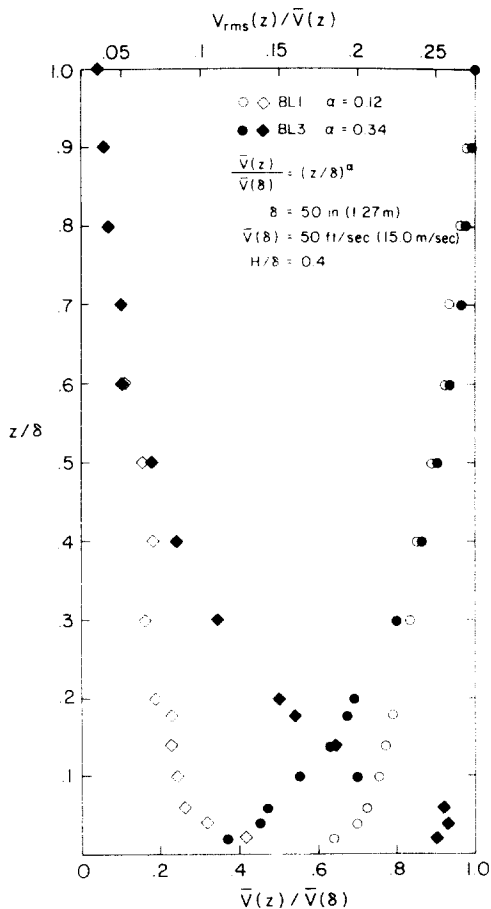
Fig. 2. Mean-velocity and turbulence-intensity profiles; ○, ●, BL1 and BL3 mean velocities; ◇, ◆, BL1 and BL3 turbulence intensities.
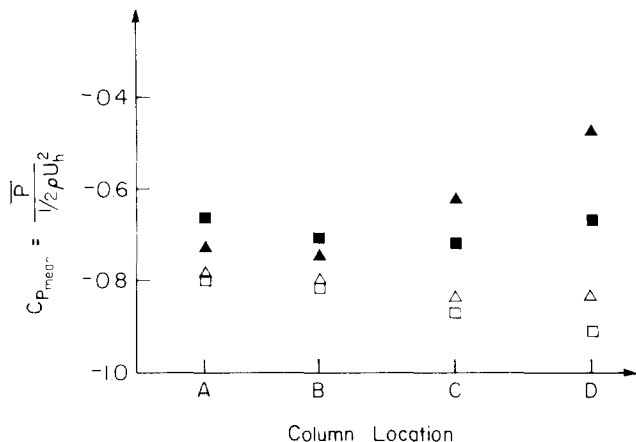
Fig. 3. Distributions of mean-pressure coefficients at levels 2 and 3: $\square$, $\triangle$, BL1; $\blacksquare$, $\blacktriangle$, BL3.
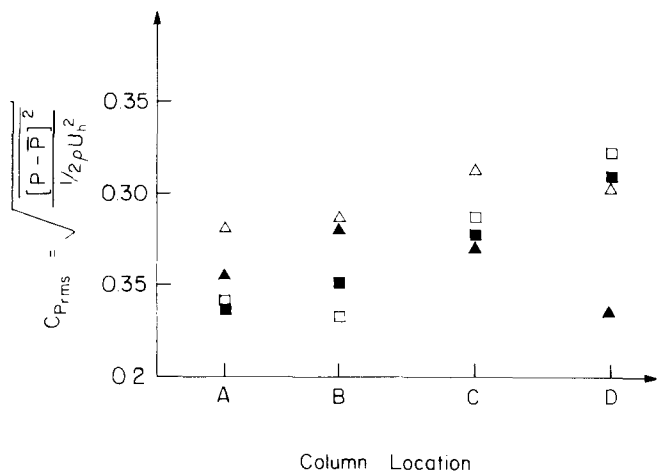

Fig. 4. Distributions of r.m.s. pressure coefficients (for key to symbols, see caption to Fig. 3).

No blockage correction has been applied to these values, because blockage was small and the flexible roof of the tunnel was adjusted to remove the longitudinal pressure gradient in the tunnel (model area/tunnel area = 0.0192). Figure 5(a) and (b) shows the time histories of pressure fluctuations measured simultaneously at six levels for the taps located on columns A and D, respectively.

The normalized reduced power spectral density $(nS(n)/\sigma^2)$ plots are presented in Figs. 6—9 for all the taps at levels 2 and 3 for BL1 and BL3 flow conditions. The autocorrelation functions for taps located on columns
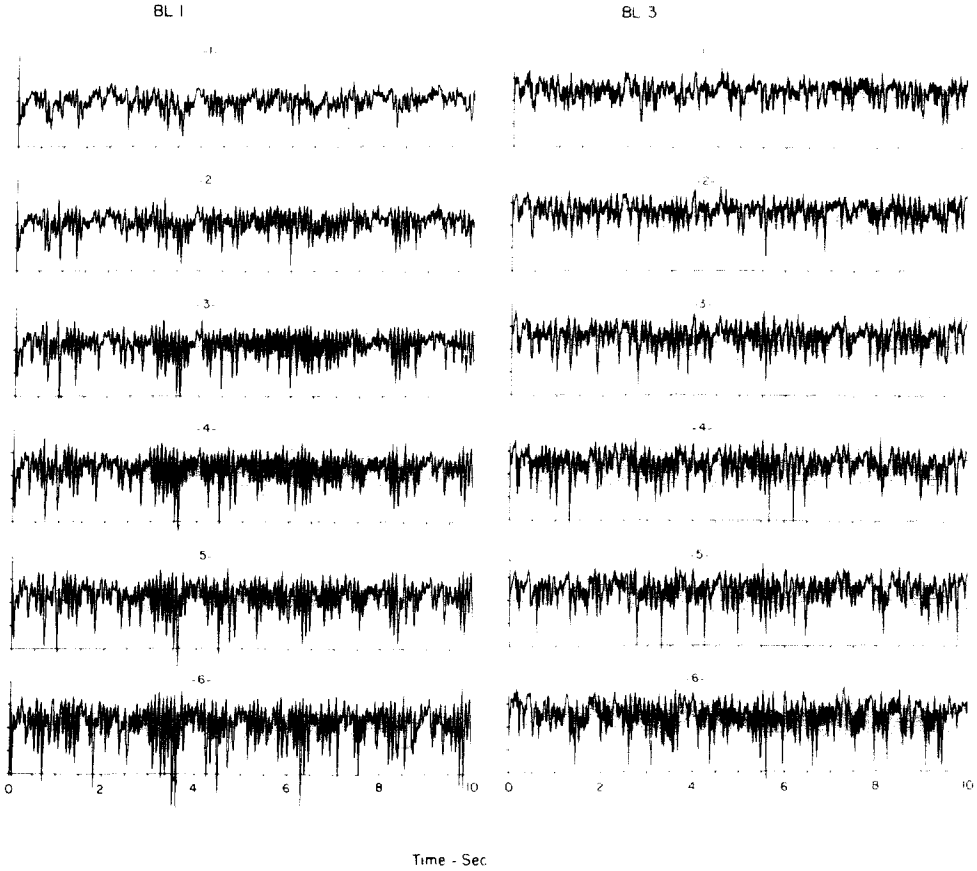
24

Fig. 5. Time histories of pressure fluctuations at levels 1, 2, 3, 4, 5 and 6 in BL1 and BL3, for taps located on (a) column A and (b) column D.

A and D at levels 2 and 3 are presented in Figs. 10 and 11. The co-spectral density function was computed for the taps located in the chordwise and spanwise directions. Figures 12—15 include the normalized co-spectra $Co(g_1, g_2, n)/[S(g_1, n) S(g_2, n)]$ between spanwise locations on columns A and D, and between chordwise locations at level 3, for the BL1 and BL3 flows. In Figs. 16—21 the cross-correlation coefficients at zero time lag are plotted as functions of the nondimensional separation distances in the chordwise and spanwise directions. In all these figures the first tap location corresponds to $X1$ and $Z1$, and only $X2$ (chordwise) and $Z2$ (spanwise) are systematically varied. The cross-correlation of the longitudinal component of the velocity fluctuations is plotted in Fig. 20 for the BL1 flow. Correlation length scales were calculated for the spanwise and chordwise directions and are reported in Table 1.

BL 1

BL 3

Time - Sec.
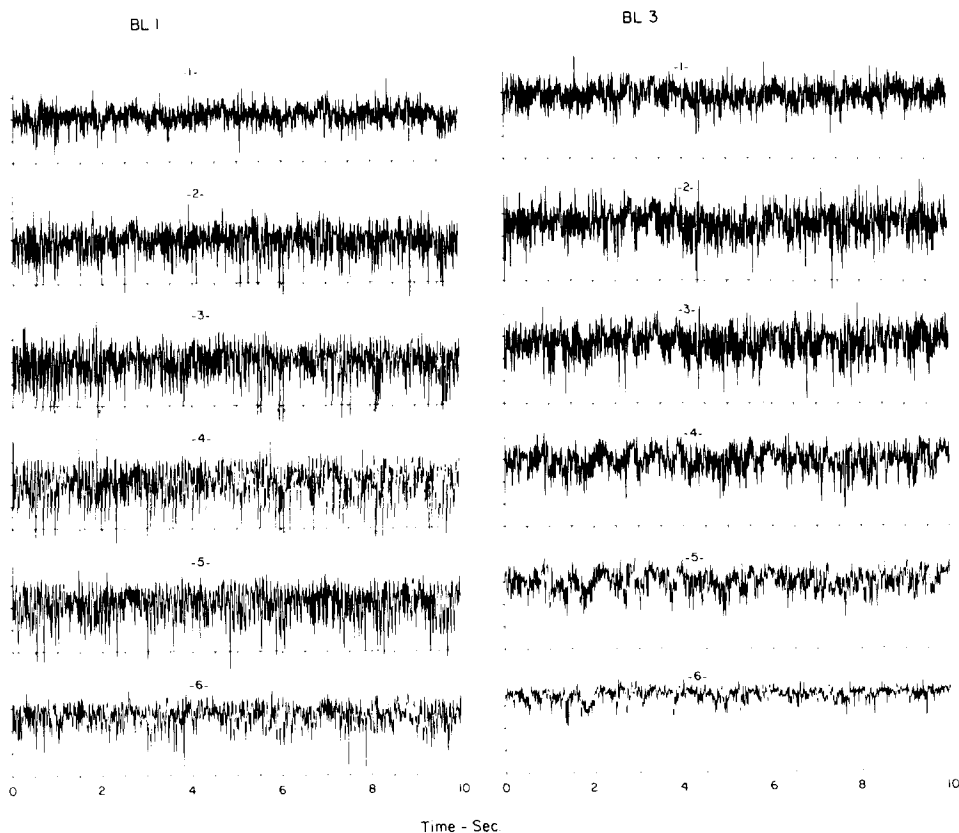
Segmental fluctuating lift-force coefficients, normalized with respect to U_h, were computed at each level from chordwise correlation matrices [8, 10]. For the overall prism lift force, coefficients were obtained from the spanwise and chordwise cross-correlation matrices. Results for the segmental and overall force coefficients are reported in Table 2. Mean square band-widths were computed to estimate the relative widths of the spectral curves for pressure taps at levels 2 and 3. The results are reported in Table 3. The cross-correlation matrices were decomposed by the extremum principle into their orthonormal eigenfunctions in the chordwise and spanwise directions. Eigenvalues for the pressure fluctuations at various levels are reported in Table 4. Relative measures of the stochastic dependence of the pressure fluctuations were derived, for selected locations, from the probability-density histograms and joint probability-density matrices.
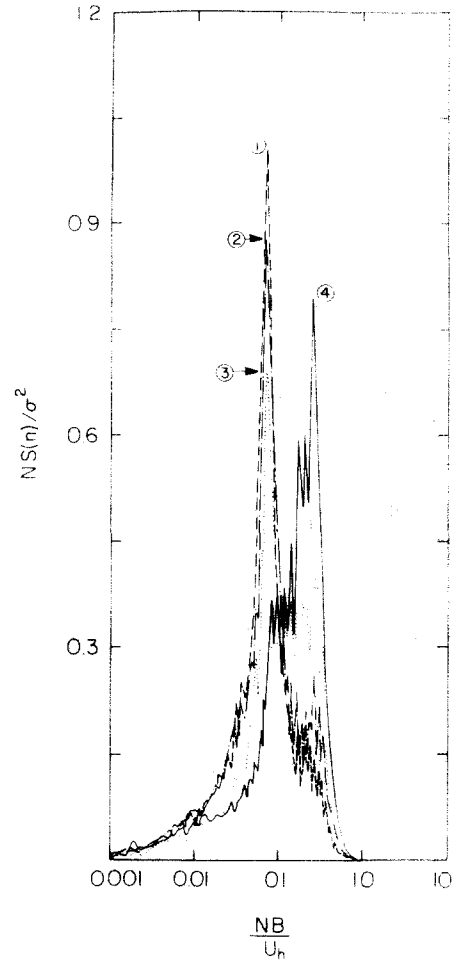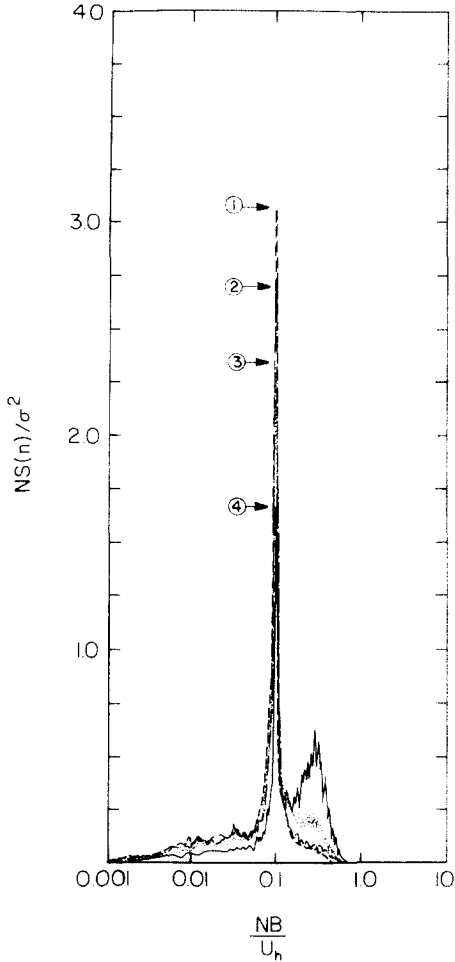
Fig. 6. Reduced power spectral densities of pressure fluctuations for BL1, level 2: tap 1-2-A,— —, ① ; tap 1-2-B,-------, ② ; tap 1-2-C, — · —, ③ ; tap 1-2-D,———, ④.

Fig. 7. Reduced power spectral densities of pressure fluctuations for BL3, level 2 (for key to symbols, see caption to Fig. 6).

4. Discussion

The nature of the fluctuating pressures on the side faces of a prismatic building model exposed to a fluid stream depends upon two basic parameters that affect the flow about the model. For a square model, these parameters are the nature of the incident flow and its angle with respect to the side faces. These basic parameters influence the modifications which take place in the structure of the separated shear layers. Consequently, the boundaries of
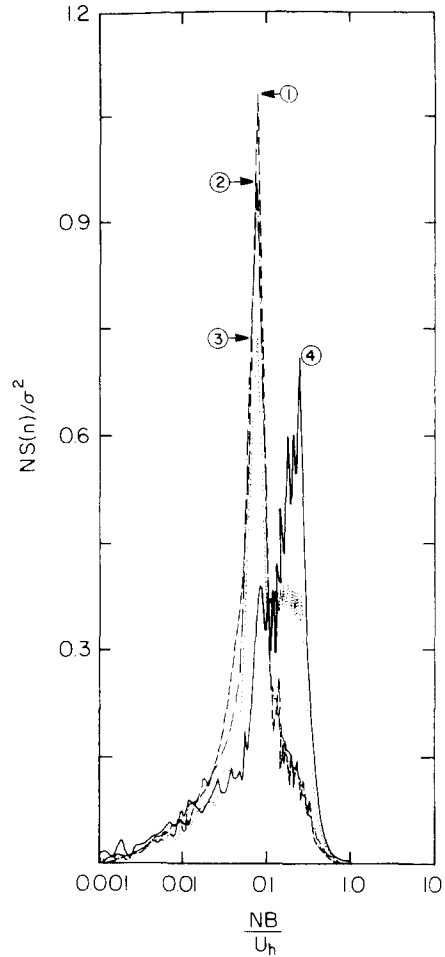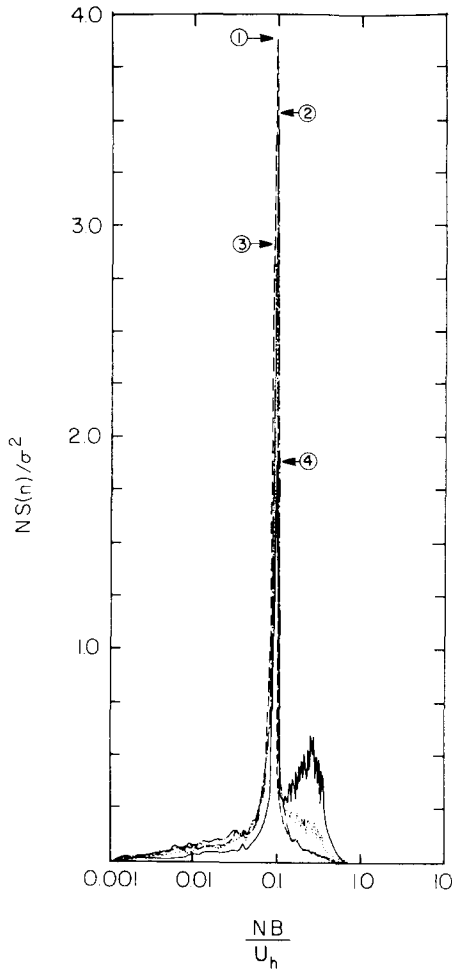
Fig. 8. Reduced power spectral densities of pressure fluctuations for BL1, level 3: tap 1-3-A,— —, ① ; tap 1-3-B,— · —, ② ; tap 1-3-C,-------, ③ ; tap 1-3-D,———, ④.

Fig. 9. Reduced power spectral densities of pressure fluctuations for BL3, level 3 (for key to symbols, see caption to Fig. 8).

the reattachment regions on the model side faces are influenced. In the following Section, a discussion is presented of the influence of the BL1 and BL3 flow characteristics on the pressure fluctuations on the side faces of a square model and their spatial correlations for 0° angle of attack.

The pertinent parameters commonly used to describe the basic characteristics of atmospheric boundary layers are illustrated in Fig. 2. In the BL1 flow there is less variation of the incident mean velocity along the model height accompanied by a lower intensity of turbulence in comparison with
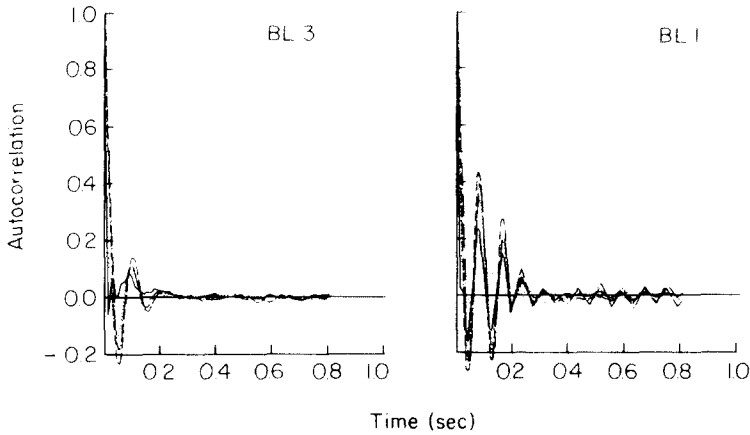
Fig. 10. Normalized autocorrelation of pressure fluctuations at level 2 (for key to symbols, see caption to Fig. 6).
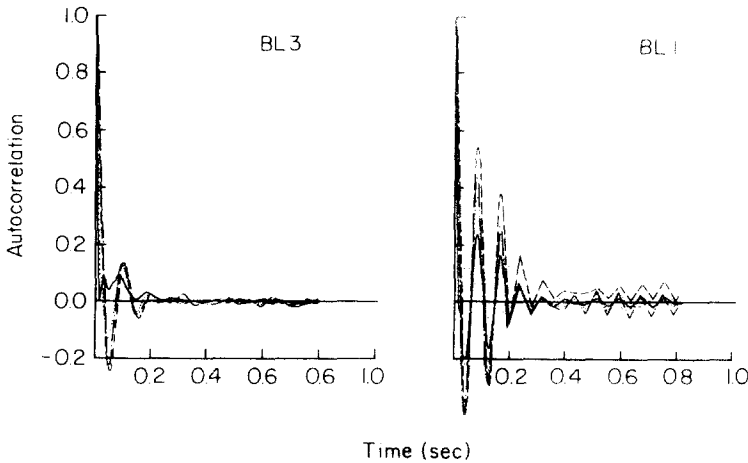

Fig. 11. Normalized autocorrelation of pressure fluctuations at level 3 (for key to symbols, see caption to Fig. 6).

BL3. For this reason, it was difficult to identify individually the influences of shear and turbulence intensity in the approach flow on the nature of the pressure fluctuations.

Addition of turbulence in the approach flow acts as a modifier of the mean flow and of wake fluctuations. An increase in the turbulence intensity of the

Fig. 12. Normalized spanwise co-spectral distributions with respect to tap 1-1-A: 1, tap 1-2-A; 2, tap 1-3-A; 3, tap 1-4-A; 4, tap 1-5-A; 5, tap 1-6-A.

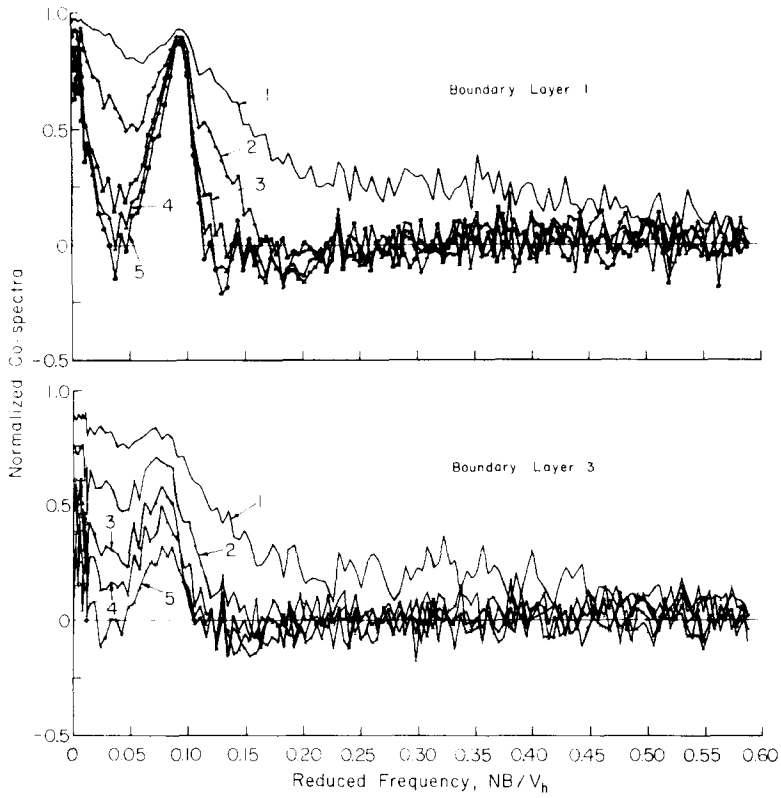Fig. 13. Normalized spanwise co-spectral distributions with respect to tap 1-1-D: 1, tap 1-2-D; 2, tap 1-3-D; 3, tap 1-4-D; 4, tap 1-4-D; 5, tap 1-6-D.
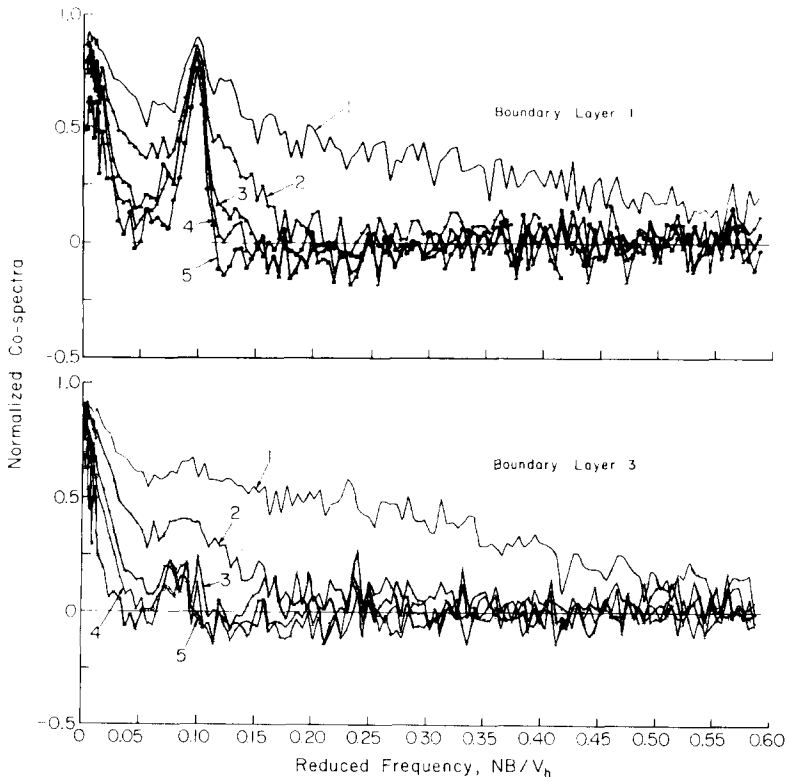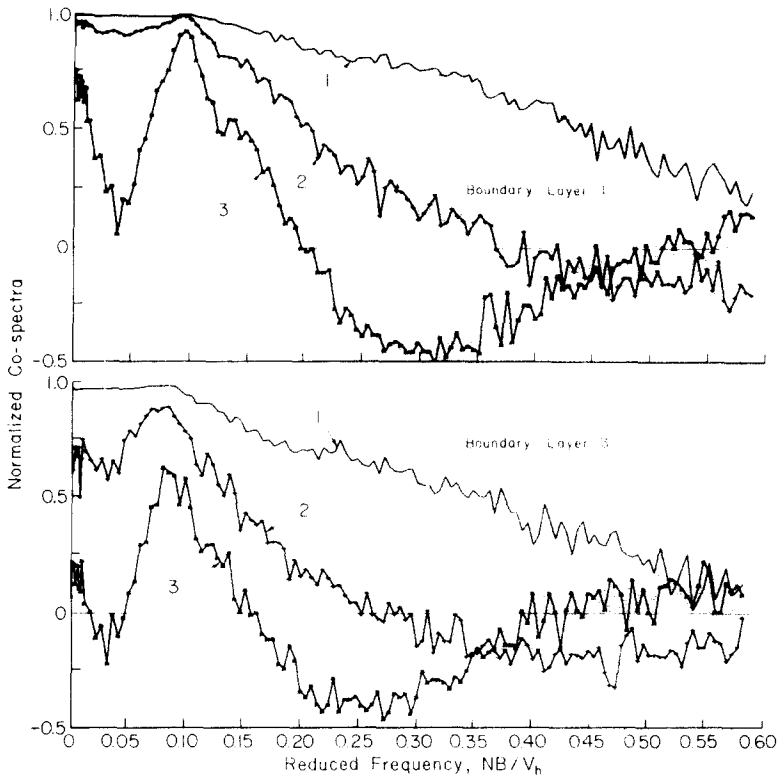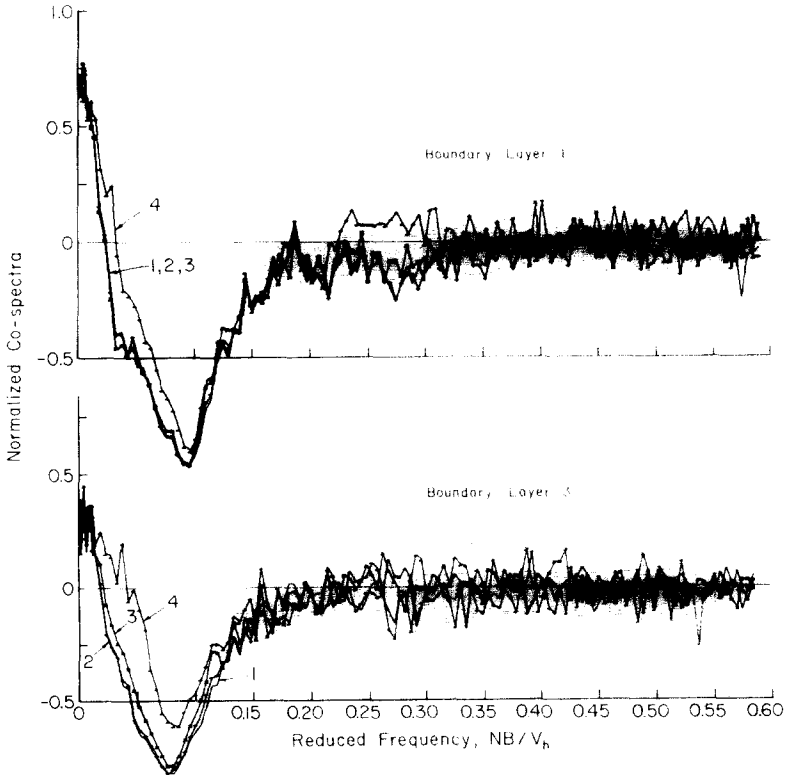
Fig. 12.

Fig. 13.

Fig. 14.

Fig. 15.

Fig. 16. Chordwise correlation-coefficient distributions with respect to the taps on column A at respective levels, in BL1 flow: △, level 1; ○, level 2; 0, level 3; □, level 4; ▽, level 5; △ , level 6; ◆, Vickery [1]; ●, Chaplin [2].

Fig. 17. Chordwise correlation-coefficient distributions with respect to the taps on column A at respective levels, in BL3 flow: ◆, Vickery [1] (for key to other symbols, see caption to Fig. 16).

approach flow promotes the entrainment process which attracts the separated shear layers to the side of the model, and thereby enhances intermittent reattachment of the flow to the side faces. This reattachment process is further enhanced in the case of models whose streamwise dimension exceeds their width. Besides the potential for reattachment, the addition of turbulence

Fig. 14. Normalized chordwise co-spectral distributions with respect to tap 1-3-A: 1, tap 1-3-B; 2, tap 1-3-C; 3, tap 1-3-D.

Fig. 15. Normalized chordwise co-spectral distributions with respect to tap 1-3-A: 1, tap 3-3-A; 2, tap 3-3-B; 3, tap 3-3-C; 4, tap 3-3-D.
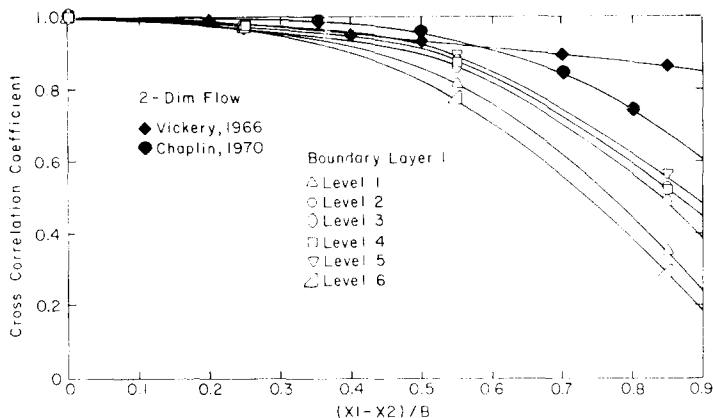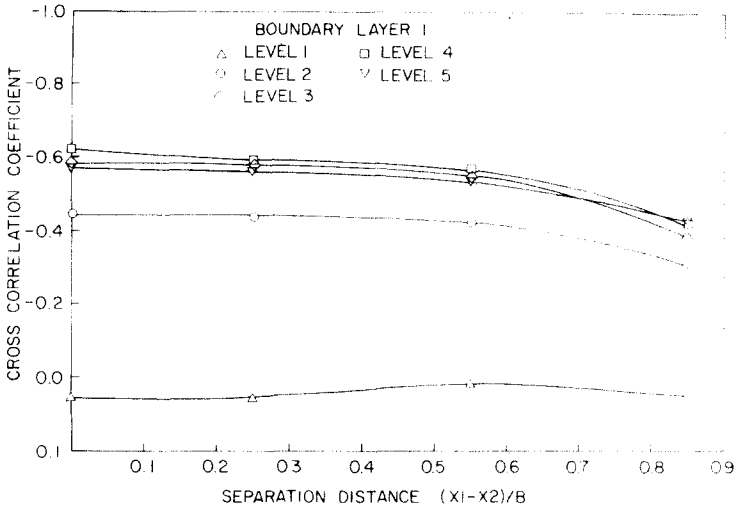
Fig. 18. Interface chordwise correlation-coefficient distributions with respect to the taps on column A at respective levels, in BL1 flow: △, level 1; ○, level 2; ◊, level 3; □, level 4; ▽, level 5.

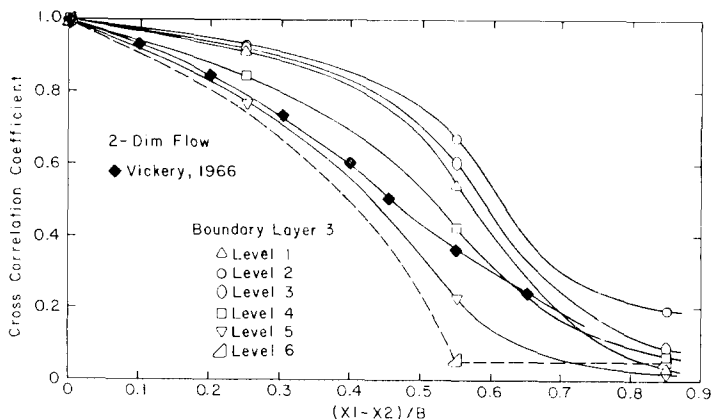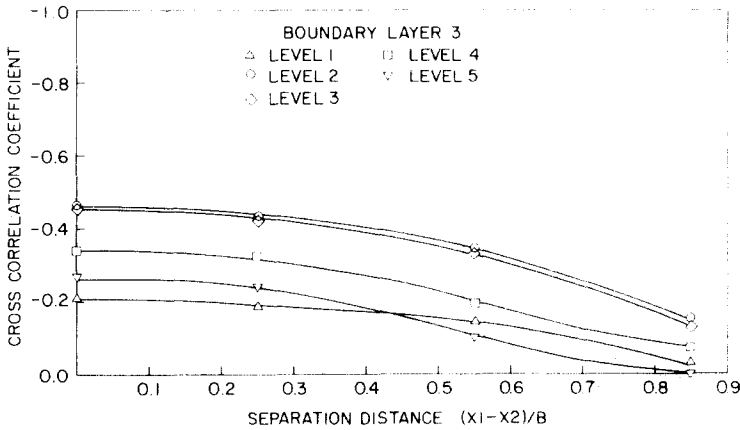Fig. 19. Interface chordwise correlation-coefficient distributions with respect to the taps on column A at respective levels, in BL3 flow (for key to symbols, see caption to Fig. 18).

promotes downstream movement of the vortex-formation region. This results in the formation of weaker vortices further downstream, thus encouraging pressure recovery on the side faces. In Fig. 3 the mean pressure distribution on the side faces of the model indicates that an increase in the turbulence intensity of the approach flow promotes pressure recovery towards the downwind regions of the side faces. A general increase in the r.m.s. values of the pressure coefficients near the downwind end of the side face is shown in Fig.
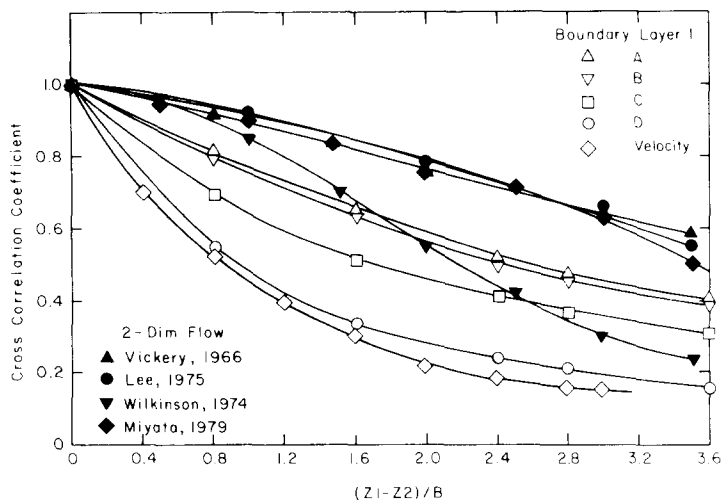
Fig. 20. Spanwise correlation-coefficient distributions with respect to the taps at level 1 for respective columns, in BL1 flow: △, column A; ▽, column B; □, column C; ○, column D; ◇, spanwise velocity fluctuations; ▲, Vickery [1]; ●, Lee [4]; ▼, Wilkinson [3]; ◆, Miyata and Miyazaki [5].
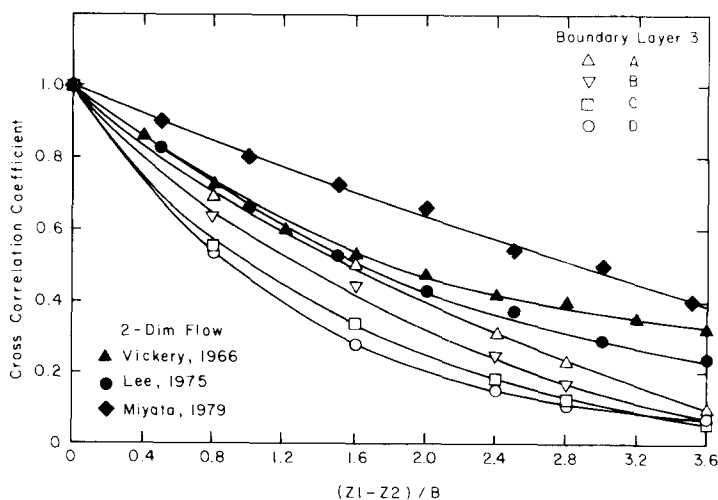
Fig. 21. Spanwise correlation-coefficient distributions with respect to the taps at level 1 for respective columns, in BL3 flow (for key to symbols, see caption to Fig. 20).

4, reaching a maximum at the reattachment point. Akins [6] observed a similar effect of incident turbulence intensity on the reattachment of flow on the side faces of a square cross-section model in a series of atmospheric boundary layers. For the approach flow with the lowest level of turbulence intensity, no reattachment was observed for a wind direction of 0°. As the turbulence

TABLE 1

Correlation length scales

Spanwise

Column	Flow	
	BL1	BL3
A	2.12*B*	1.71*B*
B	2.06*B*	1.50*B*
C	1.93*B*	1.31*B*
D	1.42*B*	1.21*B*
Average	1.88*B*	1.43*B*

Chordwise

Level	Flow	
	BL1	BL3
1	0.715*B*	0.540*B*
2	0.735*B*	0.600*B*
3	0.755*B*	0.578*B*
4	0.766*B*	0.494*B*
5	0.780*B*	0.410*B*
6	0.680*B*	0.370*B*
Average	0.74*B*	0.5*B*

TABLE 2

R.m.s. force coefficients

Segmental coefficients

Level	Flow	
	BL1	BL3
1	0.22	0.23
2	0.35	0.32
3	0.42	0.33
4	0.46	0.33
5	0.47	0.27
Overall prism coefficients	0.34	0.27

TABLE 3

Mean square bandwidths

Tap	Flow	
	BL1	BL3
1-2-A	3.92	12.00
1-2-B	4.36	13.71
1-2-C	5.19	17.64
1-2-D	7.27	31.25
1-3-A	3.09	11.01
1-3-B	3.48	12.30
1-3-C	4.17	16.00
1-3-D	6.35	34.70

TABLE 4

Eigenvalues of pressure fluctuations

Level	Percentage contribution of nth eigen value, $\lambda^{(n)}/\Sigma\lambda^{(n)}$								Percentage total contribution of first four eigenvalues
	$n = 1$	$n = 2$	$n = 3$	$n = 4$	$n = 5$	$n = 6$	$n = 7$	$n = 8$	
Boundary layer 1									
1	39.34	35.64	9.40	9.31	2.98	2.83	0.25	0.22	93.69
2	54.60	23.24	8.99	8.40	1.63	1.51	1.45	0.18	95.23
3	58.68	18.79	10.00	8.69	1.67	1.52	0.28	0.25	96.16
4	63.50	17.83	8.13	6.61	1.65	1.56	0.34	0.32	96.07
5	64.00	18.72	7.11	6.85	1.50	1.44	0.18	0.18	96.68
Boundary layer 3									
1	34.68	24.10	12.59	12.56	7.22	7.05	0.92	0.89	83.93
2	40.50	20.63	15.93	13.46	4.45	3.96	0.59	0.57	90.52
3	39.40	17.87	15.60	14.55	5.68	5.15	0.88	0.85	87.42
4	34.18	19.52	15.20	10.65	8.43	7.73	1.66	1.61	79.55
5	31.75	20.10	11.74	10.66	10.20	9.96	2.85	2.74	74.25

intensity increased, reattachment on the side faces was initiated and the reattachment location moved closer to the leading edge of the model as the turbulence intensity increased. The r.m.s. lift-force coefficients reported in Table 2 are of greater magnitude for BL1 in comparison with BL3, which further emphasizes the influence of turbulence on the flow about the building model and the associated reduction in the fluctuating lift force.

4.1. Time histories

Time histories of simultaneously monitored pressure fluctuations can provide insight into the spatial extent of a possible coherent structure in the pressure field. In Fig. 5(a) and (b) the time histories of the pressure fluctuations at tap locations on columns A and D (Fig. 1) are presented for the BL1 and BL3 flows. The simultaneous occurrence of pronounced spikes in the time histories for the taps at column A suggests a coherent nature for the pressure fluctuations in the separation bubble. In the case of the BL3 flow there is less evidence of such coherent fluctuations. An increase in the freestream turbulence increases mixing in the separated shear layers and the rate of entrainment of surrounding fluid, which tend to thicken the shear layers. The lower pressure due to entrainment causes a decrease in the radius of curvature of the shear layers and thus encourages the shear layers to reattach intermittently to the rear of the side face. Therefore, the time histories for the region of reattachment (column D) exhibit more pronounced, isolated spikes and high-frequency components (Fig. 5(b)). Melbourne [11] presented a similar explanation for the behavior of separated shear layers.

4.2. Spectral analysis

A high-amplitude spike around a reduced frequency of 0.1, which corresponds to the Strouhal frequency, is a typical characteristic for the measured spectral representations. The spectral peaks are narrower and more pronounced in the case of the BL1 flow. It is shown in Figs. 6—9 that a reduction in amplitude of the spectral peaks takes place as the downwind edge of the side face is approached. This trend is present at all the levels and for each of the two approach flows. The reduction of the vortex-shedding peak amplitude is explained partly by the redistribution of energy to a wider bandwidth. This is obvious for the taps located near the downwind edge of the model side faces, which exhibit a concentration of energy at a frequency higher than the Strouhal frequency. This feature is more pronounced in the BL3 flow (Figs. 7 and 9), suggesting a possible reattachment of the separated shear layer on the downwind region of the side faces. A similar trend was indicated by the spatial distribution of the fluctuating-pressure coefficients. Lee [4] also observed that the magnitude of the spectral peak falls off sharply as the rear end of the side face is reached. Therefore, at similar tap positions in two different incident flows, with an increase in the incident flow turbulence there is a concomitant decrease in the spectral peaks. The mean square bandwidths of the spectral curves were computed in order to quantify the relative changes in spectral width. These estimates were made by equating the area under a spectrum to a rectangular area with height equal to the peak spectral amplitude and width given by the mean square bandwidth. The results presented in Table 3 reaffirm the earlier statement regarding the redistribution of energy to a wider band as the pressure-tap location approaches the downwind edge of the side face. The addition of turbulence also promotes a similar increase in the spectral width for all tap locations.

The autocorrelations of the pressure fluctuations reveal distinct oscilla-
tions in the case of BL1, which correspond to a sharp peak in the spectra,
whereas for the BL3 flow the oscillations in the autocorrelations represent
a wide-band process with higher damping (Figs. 10 and 11). Mujumdar and
Douglas [12] measured the autocorrelation function for velocity fluctua-
tions in the near-wake of a square prism in two-dimensional flow. In the
absence of turbulence-generating grids, the autocorrelation function was
characterized by the oscillations at the Strouhal frequency. However, intro-
duction of turbulence upstream of the prism exhibited a tendency to dampen
these oscillations, which agrees qualitatively with the results for the pressure
fluctuations reported in this paper.

4.3. Co-spectral analysis

The important features of the spanwise co-spectra between locations on
columns A and D are presented in Figs. 12 and 13 (time histories presented
in Fig. 5(a) and (b)). The plots are exponentially decaying functions of re-
duced frequency, with a peak related to vortex shedding at the Strouhal
frequency. The spectral energy arising from vortex shedding is more pro-
nounced in the case of taps located at column A, which are closer to the lead-
ing edge, than for taps on column D, which are nearer the downwind edge of
the side face. Addition of turbulence causes primarily a broadening and re-
duction of the shedding peak amplitude. The chordwise variation of the co-
spectra between taps at level 3 located on the same face is presented in Fig. 14;
in Fig. 15 the co-spectra between taps located on opposite-side faces are
presented. In Fig. 15 the shedding peak is negative, because of the antisym-
metric nature of vortex shedding. The nonhomogeneous nature of the pressure
fluctuations and the presence of peaks associated with vortex shedding in-
hibited quantification of the co-spectral plots into coherence exponents.

4.4. Cross-correlation

In Figs. 16—19, intraface and interface chordwise (circumferential) descrip-
tions of the cross-correlation coefficients at zero time lag are plotted for the
BL1 and BL3 flows. There is a higher rate of decay of the correlation function
for the BL3 flow. Better correlation is exhibited by the levels which are lo-
cated away from the top and bottom of the model. This trend can be explain-
ed by the presence of three-dimensionality in the flow, which promotes an
influx of fluid from the top and pronounced shear and high turbulence in-
tensity near the bottom of the prism, leading to poor correlations at levels
near the top and bottom of the prism. Results from experiments by Vickery
[1] and Chaplin [2] in two-dimensional flow are also plotted. The cross-corre-
lation between two locations at the same level, but located on opposite-side
faces, has a negative value (Figs. 18 and 19). This is due to the antisymmetric
nature of the vortex-shedding process, which is vitiated in the presence of
high levels of turbulence in the incident flow (Fig. 19), indicating a generally
lower level of energy associated with the wake fluctuations. Similar conclu-

sions were derived by Lee [4]. The average value of the correlation length scale for pressure in the chordwise direction in BL1 flow is 0.74B, which is reduced to 0.5B in BL3 (B represents the prism width).

In Figs. 20 and 21 spanwise (axial) correlations are presented for the BL1 and BL3 flows. The correlations obtained by Vickery [1], Lee [4], Wilkinson [3] and Miyata and Miyazaki [5] are also plotted, indicating correlations generally higher than the results of this study, which is attributable to the lack of three-dimensionality, absence of shear in the incident flow and other variations in the statistical characteristics of the approach flows in the former cases. Addition of turbulence in the approach flow (BL3) results in rapid decay of the spanwise correlations. The spanwise correlations on the side faces are very pronounced at column A, which is nearest to the separation edge, whereas in the region of the rear corner (column D) less evidence of correlation is exhibited. There is intermittent reattachment of the shear layers in the region of the downwind end of the side face, causing pressure fluctuations which are poorly correlated despite the overall cyclic pattern of vortex shedding. Lee [4] suggested that since the shear layers contain large, high-frequency instabilities, intermittent reattachment of shear layers to the side faces should be expected with poorly correlated pressure fluctuations despite the periodic shedding of vortices. The average values of the correlation length scales for the spanwise direction are 1.88B and 1.43B for BL1 and BL3, respectively. Information regarding the pressure-correlation length scales can be a useful input for cladding design. The results in Table 1 indicate that the length scales at different generators (columns) on the side faces of a square cross-section prism are dependent on their location relative to the leading edge, i.e., the maximum length scale corresponds to the axis closest to the separation edge. Wilkinson et al. [13] reported a similar trend. The coherent pressure fluctuations in the separation bubble exhibit higher correlation in comparison with the spanwise velocity correlation of the streamwise component for the BL1 flow (Fig. 20). The pressure correlation at column D is similar to that of the approach flow (Fig. 20), suggesting that the fluctuations in the approach flow have a significant influence on the reattachment patterns and fluctuations in the shear layer far from the separation point. A quest for a viable transfer function for the streamwise fluctuations in the approach flow and the pressure fluctuations on the side faces should provide a challenging line of research.

4.5. Eigenfunction analysis

The statistical analysis of the spatio-temporal variations in the pressure fluctuations suggests that they are nonhomogeneous, which implies their dependence not only on the separation distance and time but also on relative location on the prism face. The nonperiodic pressure field on the side faces could be decomposed by an extremum principle into its orthonormal eigenfunctions [4, 8, 14]. The integral of the mean square pressure fluctuations around the circumference of a prism at any level is equal to the sum of the

eigenvalues, and each eigenvalue represents the energy contained in its associated spatial eigenfunction [8]. The effects of added turbulence can be identified by the energy decomposition among the various spatial eigenfunctions. Eigenfunction analysis of the pressure fluctuations is reported in Table 4, which indicates that a major portion of the energy is associated with the first or fundamental eigenfunction, which is antisymmetric with respect to the side faces. This is a typical pattern for the vortex-shedding mode associated with the Strouhal frequency. The trend is more pronounced in the BL1 flow, where the energy is concentrated mainly in the fundamental eigenfunction, whereas the energy is redistributed in the higher modes for the BL3 flow, with a higher concentration remaining in the fundamental mode. Similar observations were made on the basis of the spectral analysis: i.e., in BL1 flow the pressure spectra are characterized by a sharp peak at the Strouhal frequency, whereas in BL3 there is broadening and reduction in the spectral peak at the Strouhal frequency, and additional evidence for energy at frequencies higher than the Strouhal frequency is present. Lee [4] observed a similar trend and concluded that the fundamental eigenfunction depicts the vortex-shedding mode and the associated energy is reduced when the turbulence intensity of the incident flow is increased.

4.6. Statistical dependence

Probability-density histograms and joint probability-density matrices were computed for determining a quantitative measure of statistical dependence for the pressure fluctuations at different tap locations [8]. The joint probability-density function (JPDF) for stochastically independent processes can be factored into two individual probability-density functions (PDF's). Thus, the relationship $P_{ij}(x, y) = P_i(x)P_j(y)$ can be used as a definition for stochastic independence, since this factorization is both a necessary and sufficient condition. The normalized deviation between the product of the individual probabilities and the joint probability density was computed as a quantitative measure of dependence. It is defined as

$$\hat{\sigma}_P = \left\{ \sum_{ij} \sum \sum [P_i(x)P_j(y) - P_{ij}(x, y)]^2 dx dy / \sum \sum [P_{ij}(x,y)]^2 dx dy \right\}^{1/2}$$

and represents the relative volume that lies between the two surfaces generated by the product of the PDF's and by the JPDF [8]. The normalized deviations $\hat{\sigma}_P$ for the pressure fluctuations at taps 1-2-A and 1-2-D are 0.48 and 0.37 in the BL1 and BL3 flows, respectively. These values suggest that the fluctuations at columns A and D are relatively more dependent in BL1 compared with BL3 flow. In the spanwise direction the normalized deviations at taps 1-2-A and 1-5-A are 0.5 and 0.38 in the BL1 and BL3 flows, respectively. These results indicate that the addition of turbulence affects the spatial dependence of the pressure fluctuations in both the spanwise and chordwise directions.

5. Conclusions

The experimental measurements reported herein lead to several conclusions regarding the nature of the pressure fluctuations on the side faces of a square building model in boundary-layer flows parallel to these faces, as follows.

(i) The effect of increasing the turbulence intensity in the incident boundary layer flow is to induce early reattachment and associated pressure recovery on the side faces, resulting in reduction of the lift-force coefficient.

(ii) The effects of added turbulence on the spectral peak of the pressure fluctuations on the side faces, apart from a slight reduction in the Strouhal number, are primarily a broadening and lowering of the peak in the spectral density function. Similarly, the periodicity in the autocorrelation function is damped as a consequence of added turbulence in the approach flow.

(iii) The pressure fluctuations exhibit relatively higher chordwise correlations at levels away from the top and base regions of the prism. The spanwise correlations on the side faces are very pronounced in the separation bubble, whereas near the downstream edge less evidence of correlation is exhibited. This is the region of intermittent reattachment of shear layers, causing pressure fluctuations which are poorly correlated despite the overall cyclic pattern of vortex shedding. Addition of turbulence deteriorates the spanwise and chordwise correlations of the pressure fluctuations.

(iv) The pressure fluctuations on the side faces of a prism are nonhomogeneous, which implies that they are dependent not only on the separation distance and time but also on the relative location.

(v) The pressure fluctuations can be expanded into orthogonal eigenfunctions. The major portion of the fluctuating-pressure energy is associated with the first eigenfunction, which is antisymmetric and represents the vortex-shedding mode. An increase in the turbulence intensity of the incident flow results in a significant redistribution of energy to the higher modes.

(vi) Quantitative assessment of the degree of statistical dependence of the pressure fluctuations on the model surface suggests a decrease in the spatial dependence with an increase of the turbulence level in the approach flow.

Acknowledgements

References

1   B.J. Vickery, Fluctuating lift and drag on a long cylinder of square cross-section in a smooth and in a turbulent stream, J. Fluid Mech., 25 (1966) 481—494.

2   J.R. Chaplin, Flow-induced forces and wake dynamics of cylindrical bodies. Ph.D. Thesis, Department of Civil Engineering, University of Bristol, 1970.
3   R.H. Wilkinson, On vortex-induced loading on long bluff cylinders, Ph.D. Thesis, Department of Civil Engineering, University of Bristol, 1974.
4   B.E. Lee, The effects of turbulence on the surface pressure field of a square prism, J. Fluid Mech., 69 (1975) 263—282.
5   T. Miyata and M. Miyazaki, Turbulence effects on the aerodynamic response of rectangular bluff cylinders, in J.E. Cermak (Ed.), Wind Engineering, Proc. 5th Int. Conf. on Wind Engineering, Fort Collins, Co, Vol. 1, Pergamon, 1980, pp. 631—642.
6   R.E. Akins, Wind pressures on buildings, Ph.D. Thesis, Department of Civil Engineering, Colorado State University, Fort Collins, CO, 1976.
7   J.E. Cermak, Laboratory simulation of the atmospheric boundary layer, Am. Inst. Aeronaut. Astronaut. J., 9 (1971) 1746—1754.
8   A. Kareem, Wind-excited motion of buildings, Ph.D. Thesis, Department of Civil Engineering, Colorado State University, Fort Collins, CO, 1978.
9   A. Kareem and J.E. Cermak, Wind tunnel simulation of wind—structure interactions, Instrum. Soc. Am. Trans., 18 (4) (1979) 23—41.
10   A. Kareem, Fluctuating wind loads on buildings, J. Eng. Mech. Div., Am. Soc. Civ. Eng., EM6 (1982).
11   W.H. Melbourne, Turbulence effects on maximum surface pressures: a mechanism and possibility of reduction, in J.E. Cermak (Ed.,), Wind Engineering, Vol. 1, Proc. 5th Int. Conf. on Wind Engineering, Pergamon, 1980.
12   S.A. Mujumdar and W.J.M. Douglas, Autocorrelation measurements in the near wake of square cylinders in turbulent free streams, Phys. Fluids, 13 (1970) 1635—1637.
13   R.H. Wilkinson, J.R. Chaplin and T.L. Shaw, On the correlation of dynamic pressures on the surface of a prismatic bluff body, Proc. IUTAM—IAHR Symp. on Flow — Induced Structural Vibrations, 1972, Springer, Karlsruhe, Germany, 1974, pp. 471—487.
14   J.L. Lumley, The structure of inhomogeneous flows, Proc. Int. Colloq. on Fine Scale Structure of the Atmosphere and its Influence on Radio Wave Propagation, U.S.S.R. Acad. Sci., 1965.